Pitch-Catch Air-Coupled Ultrasonic Technique for Detection of Barely Visible Impact Damages in Composite Laminates

Lukasz Ambrozinski, Bogdan Piwakowski, Tadeusz Stepinski, Lukasz Pieczonka, Tadeusz Uhl

PITCH-CATCH AIR-COUPLED ULTRASONIC TECHNIQUE FOR DETECTION OF BARELY VISIBLE IMPACT DAMAGES IN COMPOSITE LAMINATES

L. Ambrozinski[1], **B. Piwakowski**[2], **T. Stepinski**[1], **L. Pieczonka**[1] **and T. Uhl**[1]

[1] *AGH University of Science and Technology, al. Mickiewicza 30, 30-059 Krakow, Poland*
[2] *IEMN École Centrale de Lille, Cedex 59-651 Villeneuve d'Ascq, France*

ambrozin@agh.edu.pl, bogdan.piwakowski@ec-lille.fr, tadstepin@agh.edu.pl, lpiecz@agh.edu.pl, tuhl@agh.edu.pl

ABSTRACT

In this paper we demonstrate an application of Lamb waves, evoked and sensed using air-coupled transducers, with the aim to detect barely visible impact damages (BVID). Experimental results, performed using a pair of air-coupled transducers operating in pitch-catch setup, are presented. In this setup, selective excitation and reception of selected Lamb wave modes is possible by changing transducers' angle of incidence. Results of scanning of a carbon-fiber reinforced polymer (CFRP) panel using S_0 Lamb wave mode are presented in the paper, and different damage detection strategies are analyzed to detect impact damages in the panel.

KEYWORDS : *Lamb waves, air-coupled ultrasound, low-energy impact damage, composite*

INTRODUCTION

SHM applications involve normally a set of actuators/sensors integrated with the investigated structure. In some cases, however, permanent installation of sensors is not feasible and instead separate structural elements have to be inspected using nondestructive testing (NDT). In these applications advanced effective NDT techniques are recommended. Automated NDT inspection, that can be performed frequently without disturbing structure's operation, is needed to minimize the necessary interrupts in structure operation. In such situations, the NDT inspections can be used as either extension or substitution of the embedded SHM systems.

Air-coupled ultrasound is a promising method which can mitigate problems related to the presence of coupling agent required for contact or immersion NDT ultrasonic inspections. Unfortunately, air-coupled ultrasound is related to other issues, which means that in many applications it cannot replace conventional ultrasound techniques. The main problem encountered when air-coupled ultrasound is used for the inspection of solid materials results form a very large impedance mismatch between solids and air, due to which only a small portion of acoustic energy emitted by the transducer can be transmitted into the investigated object. The simplest and most natural way of reducing the effects of acoustic impedance mismatch between a solid object and air is transmitting high-energy pulses and using high-gain, low-noise receiving amplifiers. Applications of high-voltage excitation [1] and effective matching layers reducing the impedance mismatch [2] have been proposed to aleviate this problem.

Two types of air-coupled transducers used in imaging applications are multilayered piezoelectric transducers and capacitive micromachined ultrasonic transducers (CMUT) [3]. Due to the mismatch problem, these transducers can only be applied in transmitter-receiver configurations, most often for the inspection of relatively thin flat panels using bulk waves in through-thickness setup [4]. This appears to be impractical in most industrial applications where only one side of the structure is accessible. Therefore, the methods that do not require the double-sided access are of great practical interest [5]. In the research presented in our previous paper [6] we investigated the pitch-catch setup, which does not have this limitation. Bulk waves cannot be used in this setup and more sophisticated surface and Lamb waves are to be considered instead. Two types of artificial damages were evaluated in our previous study [6]: a delamination, created using a Teflon film inserted during the manufacture process, and a well-visible crack of significant dimensions. We showed that these defects could be successfully detected and localized by means of Lamb waves using pitch-catch setup.

Motivated by the positive results obtained previously, in this study we use the same setup to detect barely visible impact damages (BVID), typical for composite materials. The investigated objects are in this study two CRFP plates with BVIDs obtained at impact energies of 2.1J and 3.9J. Additionally we use vibrothermography to verify the results obtained using ultrasound.

1. Theoretical background

As an introduction we briefly outline the physical principles of leaky Lamb waves generation and reception by the means of air-coupled transducers in this section. Next, the phenomena encountered during the interaction of Lamb waves with the defects specified above will be described.

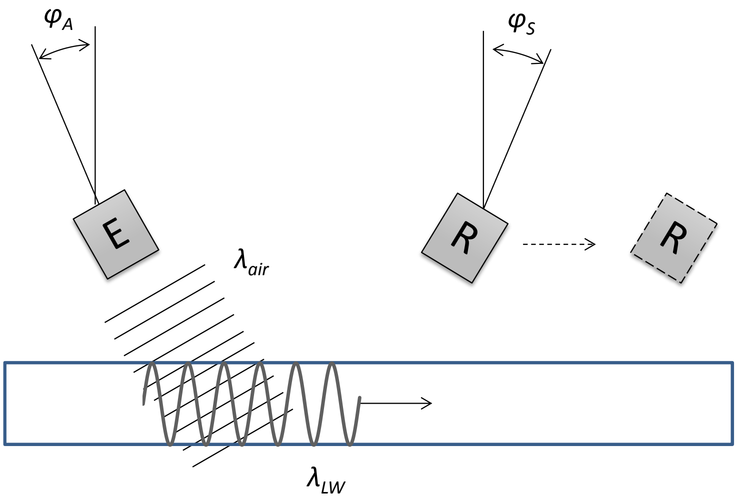

Figure 1 : Principles of Lamb waves generation and reception using air-coupled transducers

Lamb waves existing in thin plates are dispersive and multimodal, which means that an infinite number of symmetric and antisymmetric modes can exist for each frequency. Numerous Lamb modes that are present in received ultrasonic signals make its interpretation difficult and therefore, the use of mode-selective excitation and reception techniques is beneficial. A single mode excitation by means of air-coupled transducers can be performed based on the principles presented in fig. 1. In order to excite a single (or at least an enhanced) mode the incident angle of the emitter φ_A has to be set to a value which can be calculated from the Snell's law

$$\varphi_E = sin^{-1}(\frac{V_{air}}{V_{LW}}) = sin^{-1}(\frac{\lambda_{air}}{\lambda_{LW}}), \quad (1)$$

where: V_{air} denotes sound velocity in air, and V_{LW} phase velocity of the excited Lamb wave. λ_{air} and λ_{LW} denote respectively the wavelengths in air and the inspected plate. The same principle can be used to make the receiver sensitive to the selected mode (i.e $\varphi_A = \varphi_S$).

The main reason reasons for the selective excitation/reception of Lamb waves is their complex physical nature (dispersive, multimodal character) as well as that various modes are sensitive to different types of flaws [7]. Furthermore, different phenomena can occur when a Lamb wave interrogates with damage. Damage detection and characterization techniques rely on the feature extraction of the captured signals that are specific for different damage types. For instance, since a crack normally causes scattering the reflected wave can be an indicator used in a damage detection and localization procedure. Another phenomenon that may take place at a damage interface is mode-conversion, e.g., an S_0 mode incident at a defect produces an A_0 mode. Besides the mode conversion, wave energy dissipation caused by damage is a common phenomenon and therefore the analysis of the wave amplitude decay can be a valuable source of information.

2. EXPERIMENTAL SETUP

The experiments were carried out with the use of two air–coupled transducers: the emission was provided by means of a non-contact transducer NCG350-D50 with the resonant frequency of 350kHz, provided by Ultran Group, USA. The membrane type, non-contact wide band transducer type mBAT-1 manufactured by Micro-Acoustics, Canada was used as a receiver. The transducers were mounted in a precise mechanical scanner, presented in Figure 2, which was used to shift the sensor along the wave propagation path and enabled obtaining B-scan images for the each measured profile [8]. Aditionaly, the scanner gimbals facilitated adjustment of the incident angle of the transducers to excite and receive Lamb modes selectively.

A broadband linear chirp signal with the frequency band from 100 to 500kHz was used as an excitation. The received signals were then cross-correlated with the excited signal using matched filtration technique.

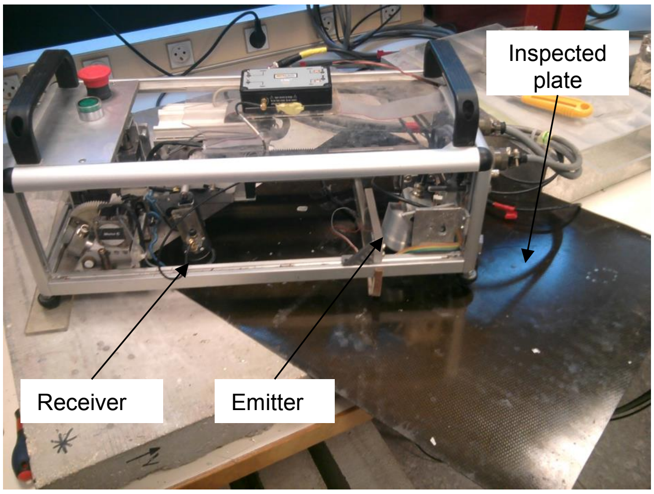

Figure 2 : Mechanical scanner used in the experiments [8].

2.1 Investigated objects

Two laminated composite plates with BVIDs were investigated. The plates were manufactured from carbon/epoxy (Seal HS160/REM) unidirectional prepreg layers. The stacking sequence of the laminate was $[0_3/90_3]_s$. The dimensions of the plates were $150 \times 300mm$, and the average laminate thickness was equal to $2mm$. Schematic diagram of the plates is shown in Figure 3. The specimens were verified free from manufacturing defects prior to testing. Low velocity impact tests were conducted on both plates to introduce damage. The plates were simply supported on a rigid post with rectangular opening

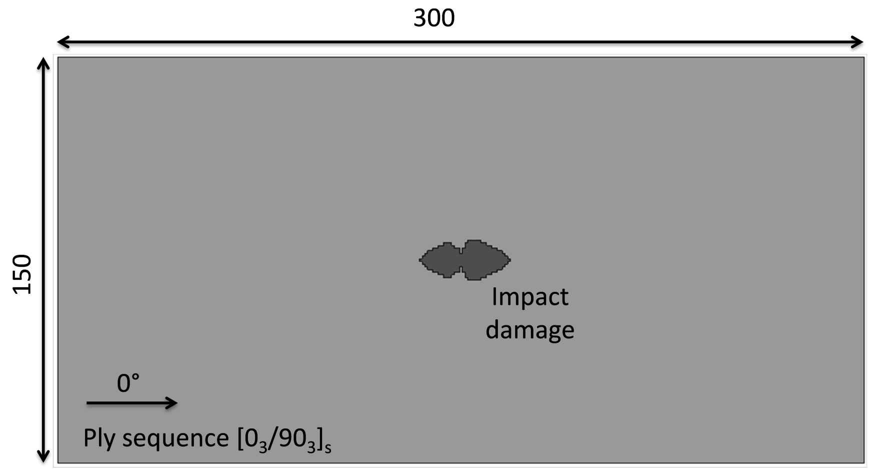

Figure 3 : Schematic diagram of the test specimen with a barely visible impact damage (dimensions are in mm).

in the center. An instrumented drop-weight testing machine was employed to impact the plates in the central location.

The two panels were impacted with different energies, respectively, 3.9J (*panel 1*) and 2.1J (*panel 2*). The desired energy levels were obtained by selecting the appropriate drop height of the impactor. The absorbed energy was evaluated by measuring the velocities of the impactor immediately before and after the impact.

After producing impacts, the extent of damage in each plate was evaluated using vibrothermography. This method is classified in the group of active thermographic nondestructive testing (TNDT) methods with external excitation [9, 10].

In vibrothermography, external energy is delivered to the structure by ultrasonic vibrations, as shown in Figure 4. Typically, a burst signal with the duration of several milliseconds is used to excite the test sample. High frequency vibrations cause energy dissipation at material discontinuities (i.e. cracks, delaminations) and mechanical energy is converted into heat. Thermographic camera is used to record the surface temperature distribution on the sample. Inference about the existence of damage is performed on the basis of the measured temperature distribution. Vibrothermography is a dark field method where the source of heat is the damage itself, which simplifies the data processing phase to a great extent.

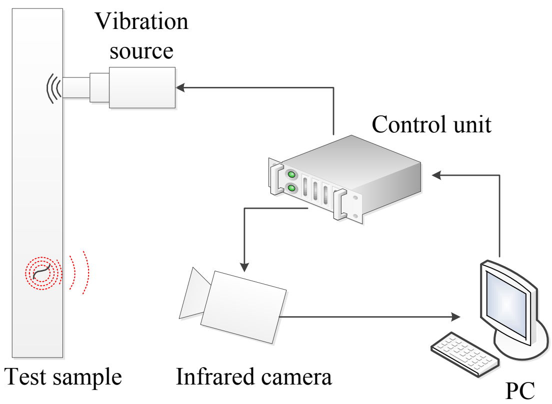

Figure 4 : Operation principle of vibrothermography [10].

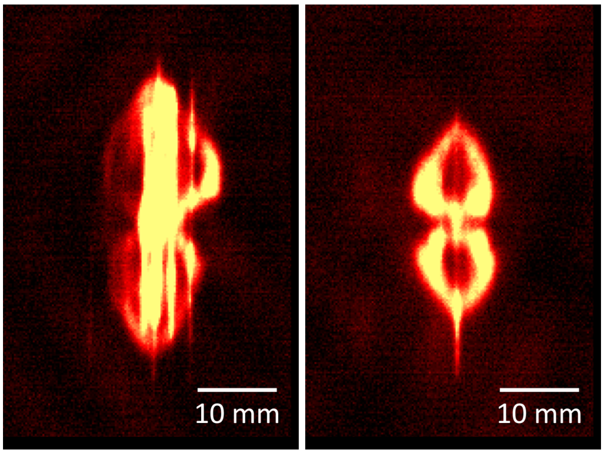

(a) (b)

Figure 5 : Results of the vibrothermographic test for the *panel 1* damaged in 3.9 J impact (a) and *panel 2* damaged in 2.1 J impact (b).

For the present investigations the Monit SHM mobile vibrothermographic test system, developed at our university, using the $35kHz$ ultrasonic excitation column was used [11]. Cedip Silver 420M photon detector camera was used to acquire thermal image sequences. The tests for both plates were performed according to the same measurement protocol. The ultrasonic column excited the plate for a period of $500ms$ and thermographic camera acquired the signal at $100Hz$ frame rate for 3 seconds.

Results of the vibrothermographic inspection, as temperature maps recorded $500ms$ after the start of ultrasonic excitation, are shown in Figure 5. As can be seen in Figure 5a the 3.9 J impact (*panel 1*) resulted in a characteristic butterfly like delamination on the $0°/90°$ interface further from the impact side and a long vertical surface crack. An animation of the recorded thermographic sequence reveals, firstly, the surface cracks, and subsequently a delamination under the surface.

Figure 5b shows the damage that resulted from the 2.1 J impact (*panel 2*). The same characteristic shape of the delamination and several vertical surface cracks can be identified. The area of delamination for the 3.9 J impact (*panel 1*) was approximately $300mm^2$, while the area of delamination for the 2.1 J (*panel 2*) impact was approximately $150mm^2$.

3. Damage detection results

In the following section, examples of Lamb waves interaction with defects will be illustrated using data obtained from the scan profiles presented in the form of B-scan images. The S_0 mode was excited in the experiments, since due to its dominant in-plane displacement it is expected to exhibit higher delamination sensitivity compared to A_0 mode.

3.1 Panel 1

Panel 1, impacted with energy of 3.9J, was investigated in in the pitch-catch setup where angles of the transmitter and receiver were set to 5° to excite and sense the S_0 mode. The signals were collected discrete points along the propagation path with a step of $1mm$. An example of B-scan image, captured at an undamaged part of the structure, is presented in Figure 6a. From the image it can be seen that besides the fast S_0 mode, a slow, hardly pronounced A_0 mode can be seen in the image. Since an undamaged part was scanned, the wavefront of the incident wave is not disturbed and the wave peaks and valleys take the form of straight lines (modes are indicated with arrows).

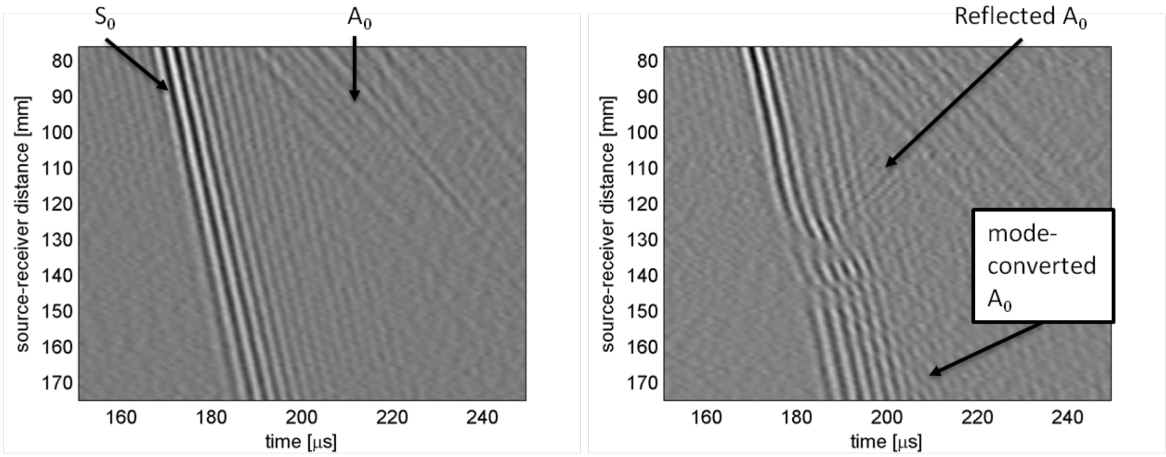

(a) (b)

Figure 6 : B–scan images representing S_0 mode propagating in non–damaged profile of *panel 1* (a) and delaminated area of *panel 1* (b)

The next scanning was performed along another profile crossing the damage. From the B–scan image, presented in Figure 6b, an interaction of the incident wave with the defect can be observed. Signal attenuation and change of slope of the incident wavefront can be seen in the damaged area. Note that although the sensor angles were not matched to the A_0 modes, weak reflected and mode-converted A_0 modes can be seen in the image.

3.2 Panel 2

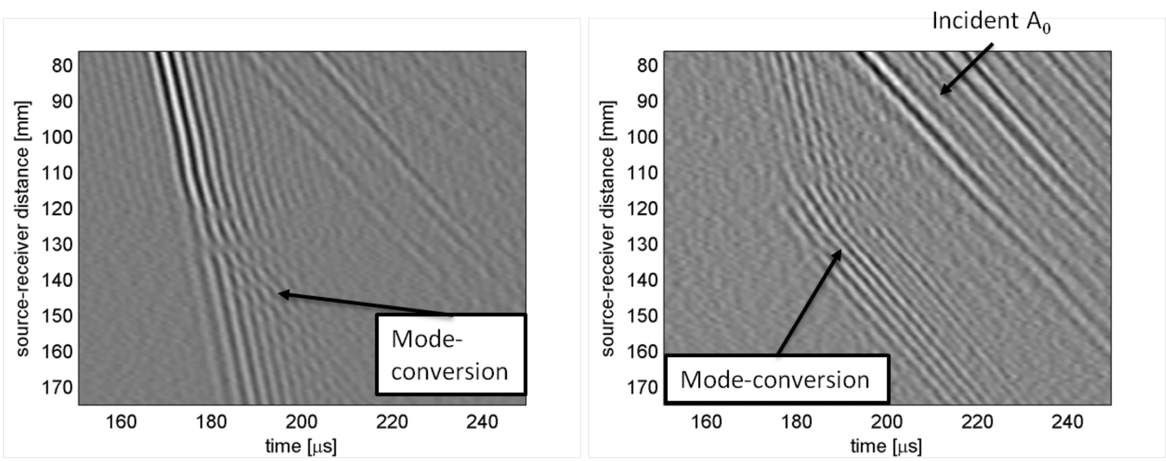

(a) (b)

Figure 7 : B–scan images representing S_0 mode propagating in delaminated area of *panel 2* (a) and $S_0 \rightarrow A_0$ mode–conversion at damage in *panel 2* (b).

In the experiment performed on the *panel 2* the setup parameters remained the same as in the former experiment. A set of profiles recorded for an undamaged area of the sample revealed, as in the previous case presented in Figure 6a, a well pronounced incident S_0, and a slightly visible A_0 mode. However, the B-scan image, captured at the damaged area, presented in Figure 7a, reveals an interaction of the S_0 mode with the defect. Slight attenuation of the propagating incident wave can be seen, and additionally the mode-converted $S_0 \rightarrow A_0$ mode can be observed. The mode-converted wave has a small amplitude since the angle of the receiver was not set to enhance this mode. Therefore, another experiment was performed to investigate the conversion more thoroughly.

In this test the angle of the emitter remained the same, i.e. 5° to excite the S_0 mode, whereas the angle of the sensor was set to 13° which allowed to enhance the A_0 mode. From the B–scan image, presented in Figure 7b, clear incident A_0 wave can be seen, which means that, although, the emitter was set to excite a single mode, in fact, both modes were evoked. Moreover, a barely visible incident S_0 mode is present, however, when the incident rapid wave reaches the damaged area it is converted to A_0 mode that is enhanced in the reception thanks to the angle of the receiver.

4. Conclusions

Examples of the interaction of S_0 mode with barely visible impact damages created by impacts with different energy were presented in the paper. Various phenomena that occur during the interaction of a Lamb wave with a defect, such as, mode conversion, mode reflection, diffraction and signal attenuation could be clearly observed in the respective B-scan images. Thus, extracting the signal features characteristic specific for the above phenomena can facilitate the detection and localization damages.

An important advantage of air-coupled transducers is their ability to excite a desired, single, or at least en enhanced wave mode. It appears however, that, the damage-related information can be carried by waves that propagate in different directions and with different velocities. Since a single receiver can normally enhance only a single, selected wave-mode, it seems that a combination of multiple receivers could benefit in superior damage detection capability. For instance, a setup including two independent receivers that would be set individually to sense attenuation of the incident wave and detect possible mode-converted waves.

Acknowledgments

The authors would like to acknowledge Professor Francesco Aymerich for providing the test samples for analysis.

References

[1] J. Salazar, A. Turo, J.A. Chavez, J.A. Ortega, and M.J. Garcia. High-power high-resolution pulser for air-coupled ultrasonic NDE applications. *Instrumentation and Measurement, IEEE Transactions on*, 52 (6):1792 – 1798, 2003.

[2] S.P. Kelly, G. Hayward, and T.E.G. Alvarez-Arenas. Characterization and assessment of an integrated matching layer for air-coupled ultrasonic applications. *Ultrasonics, Ferroelectrics and Frequency Control, IEEE Transactions on*, 51(10):1314 –1323, oct. 2004.

[3] D.W. Schindel, D.A. Hutchins, and W.A. Grandia. Capacitive and piezoelectric air-coupled transducers for resonant ultrasonic inspection. *Ultrasonics*, 34(6):621 – 627, 1996.

[4] D.W. Schindel and D.A. Hutchins. Through-thickness characterization of solids by wideband air-coupled ultrasound. *Ultrasonics*, 33(1):11 – 17, 1995.

[5] M. Castaings, P. Cawley, R. Farlow, and G. Hayward. Single sided inspection of composite materials using air coupled ultrasound. *Journal of Nondestructive Evaluation*, 17:37–45, 1998. 10.1023/A:1022632513303.

[6] L. Ambrozinski, B. Piwakowski, T. Stepinski, and T. Uhl. Application of air-coupled ultrasonic transducers for damage assessment of composite panels. In Christian Boller, editor, *Structural Health Monitoring 2012: proceedings of the sixth European workshop*, volume 1, pages 122 – 129, 2012.

[7] B. C. Lee and W.J. Staszewski. Lamb wave interaction with structural defects: modeling and simulations. In Ralph C. Smith, editor, *Proc. of SPIE*, volume 5049, pages 146–155, 2003.

[8] F. Soltani, M. Goueygou, Z. Lafhaj, and B. Piwakowski. Relationship between ultrasonic Rayleigh wave propagation and capillary porosity in cement paste with variable water content. *NDT & E International*, 54(0):75 – 83, 2013.

[9] X. Maldague. *Theory and Practice of Infrared Technology for Nondestructive Testing.* John Wiley & Sons, 2001.

[10] L. Pieczonka and M. Szwedo. *Advanced Structural Damage Detection: From Theory to Engineering Applications*, chapter Beamforming of guided waves, pages 177–210. Wiley, 2013.

[11] Monit SHM LLC . `http://www.monitshm.pl/index.php?loc=vibrothermogr`. 2012.